Nanophotonic Ion Sources

Jessica A. Stolee[a], Bennett N. Walker[a], Yong Chen[b], and Akos Vertes[a*]

[a]*Department of Chemistry, George Washington University, Washington, DC 20052, USA*
[b]*Current address: Genomics Institute of the Novartis Research Foundation, 10675 John Jay Hopkins Drive, San Diego, CA 92121*

Abstract. Interactions between laser radiation and photonic structures at elevated laser intensities give rise to the production of positive and negative ions from adsorbates. These new types of ion sources exhibit properties that are significantly different from conventional laser desorption ionization sources. In this contribution comparisons are made between matrix-assisted laser desorption ionization (MALDI) of biomolecules with ion production from laser-induced silicon microcolumn arrays (LISMA) and nanopost arrays (NAPA). The sharp increase of ion yields from the nanophotonic ion sources follow a power law behavior with an exponent of up to $n \approx 7$, whereas in the case of MALDI $n \approx 5$. The strong field enhancement in the vicinity of the columns and posts scales with their aspect ratio. Slender high aspect ratio posts show reduced laser fluence threshold for ionization. Posts with diameters at or below the thermal diffusion length demonstrate high surface temperatures due to the radial confinement of the deposited energy. As a consequence enhanced fragmentation, i.e., lower survival yield of the molecular ions is observed. The origin of protons in the ionization of adsorbates was identified as the entrapped residues of the solvent.

Keywords: photonics, laser desorption ionization, mass spectrometry, nanostructures, silicon
PACS:, 68.43.Tj, 78.67.-n, 79.20.Eb, 79.20.La, 81.07.-b, 82.80.Ms

INTRODUCTION

When a pulsed laser irradiates a solid surface, rapid energy deposition can cause mechanical, thermodynamic and chemical changes that include desorption, ablation, ionization, or a combination of these events. In laser desorption, the excitation of the substrate and/or the adsorbates results in the removal of surface monolayers.[1, 2] At higher laser fluences, microscopic volumes of material are removed by ablation and in the produced plume plasma formation can occur.[3-5]

Laser desorption from optically absorbing substrates, at 10^5-10^6 W cm^{-2} irradiance, transfers relatively little material from the solid to the vapor phase and leaves no substantial damage on the surface. Laser ablation, at 10^7-10^8 W cm^{-2} irradiance, produces a plume of atoms/molecules, ions, electrons, clusters and particulates, and leaves a crater on the affected surface of the target. Further increasing the irradiance results in plasma ignition that makes the plume opaque and leads to dramatically increased ion production accompanied by the degradation of molecules.

In both laser desorption and laser ablation, a certain fraction of the volatilized material is in the form of ions. Ion production from organic insulators, such as high

CP1278, *International Symposium on High Power Laser Ablation 2010,* edited by C. R. Phipps

molecular weight materials, is diminished by laser-induced decomposition of the molecules. Direct laser ionization of organic and biomolecules is essential for their mass spectrometric analysis.

In matrix-assisted laser desorption ionization (MALDI), a UV-absorbing matrix is used to facilitate the laser energy deposition that drives the volatilization and ionization of the embedded analyte molecules.[6, 7] A moderate laser irradiance of $\sim 10^6$ W cm^{-2} is required to produce ions in MALDI.[8] Desorption of material in MALDI occurs in a non-equilibrium phase transition and ions can be formed in the low density plume of the desorbed material.

In these conventional laser ionization sources, the interaction between the laser pulse and the target is governed by the linear and non-linear optical properties of the material. When the target is structured on the length scale of the radiation wavelength, photonic interactions emerge as the determining factor in energy deposition. Under certain conditions, interactions of the laser radiation with unstructured surfaces can create photonic structures through interference evaporation instabilities.[9] For example, laser-induced silicon microcolumn arrays (LISMA), can be produced by ultrafast laser irradiation of silicon wafers.[10-12] While the governing factors and the plume dynamics of conventional desorption and ablation are well understood, laser-induced material removal based on photonic interactions is essentially unexplored.

Initial studies indicate that photonic structures can also be utilized for ion production and, consequently, as laser desorption ionization platforms in mass spectrometry.[12] Depending on the characteristic lengths in these structures they can be termed as **photonic or nanophotonic ion sources**. While laser processed silicon has been extensively studied for sensor and energy conversion applications,[13] the laser light-nanostructure interaction regime that results in ion production has not been investigated.

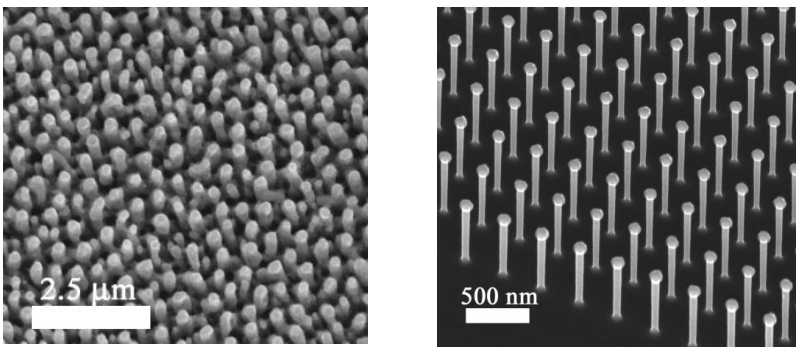

(a) **(b)**

FIGURE 1. Scanning electron microscope (SEM) image of (a) quasi-periodic LISMA with an average column diameter, D, periodicity, P, and height, H, of 400, 600, and 800 nm, respectively and (b) NAPA with D = 100, P = 337, and H = 1000 nm.

In recent studies we have demonstrated that photonic nanostructures with quasi-periodic features, such as LISMA (shown in fig. 1a), exhibit nanophotonic ion production.[14, 15] Similarly, ions can be produced from silicon nanopost arrays (NAPA) that have a well-defined periodicity, shown in fig. 1b, produced by

nanofabrication.[16] Whereas in UV-MALDI the matrix absorbs the laser energy via electronic excitation, in low resistivity silicon nanostructures it is deposited through current oscillations induced in the structure by the electromagnetic field. Our ability to tailor the dimensions of NAPA helps to reveal how the interaction between the electromagnetic radiation and the nanostructure drives ion production.

In this article we aim to characterize some salient physical properties of nanophotonic ion sources and identify the features that set them apart from other ionization platforms, e.g., MALDI.

DESORPTION BY NANOPHOTONIC INTERACTIONS

When the dimensions of a nanostructure are on the order of the wavelength of light, the evanescent components of the electromagnetic field and near-field effects need to be considered. Localization and confinement of the radiation around the nanostructure, as a result of external excitation (i.e., laser light), result in very strong near-fields. Molecules near or on the surface respond to the enhanced field by desorbing and ionizing.[17, 18]

The enhanced intensities in the vicinity of excited structures can be several orders of magnitude higher than the incident irradiance.[19, 20] For example, in the proximity of a nanoscopic silicon probe tip modeling results and molecular fluorescence experiments indicate an electric field enhancement factor, κ, of $\kappa \approx 40$, translating into a larger than 10^3-fold intensity enhancement in the near-field.[19, 21] This factor is strongly dependent on the probe tip aspect ratio and decays dramatically with the distance from the tip. For example, Bohn et al. studied the near-field enhancement factor in the vicinity of a silicon probe tip and a glass substrate.[20] Based on the electrostatic approximation that represents the local field by a point dipole and its image in the substrate, the near field intensity enhancement factor can be expressed as:

$$\kappa = 1 + \frac{8\alpha(1+\beta)}{4R_c^3 - \alpha\beta} \quad , \qquad (1)$$

where α is the tip polarizability, $\beta = (\varepsilon_s - 1)/(\varepsilon_s + 1)$, ε_s is the dielectric permittivity of the substrate and R_c is the radius of curvature of the probe tip. Eq. 1 stresses the importance of the polarizability, which is directly correlated with the radius of curvature, on the enhancement factor.

The large near-field enhancements can be partly attributed to the antenna effect due to the elongated probe. The antenna effect can be described as dependence on the length or aspect ratio of the nanostructure as well as on the polarization of the incoming electromagnetic wave.[22] Therefore, the near-field response of optical antennas can be tuned by varying the antenna dimensions or the polarization of the electromagnetic field.[23-25]

To observe the role of the antenna effect on laser desorption rates, salts of thermometer ions were deposited on NAPA structures with different post aspect ratios. The thermometer ions, such as 4-methyl-benzylpyridinium (4M), in these salts exist in the ionic form already as an adsorbate. Therefore, by observing their ion yields in their

mass spectra (see fig. 2a) we can directly monitor the desorption process, separate from the ionization step. Fig. 2b depicts the threshold fluence necessary to produce 4M ions from NAPA structures of increasing aspect ratio.

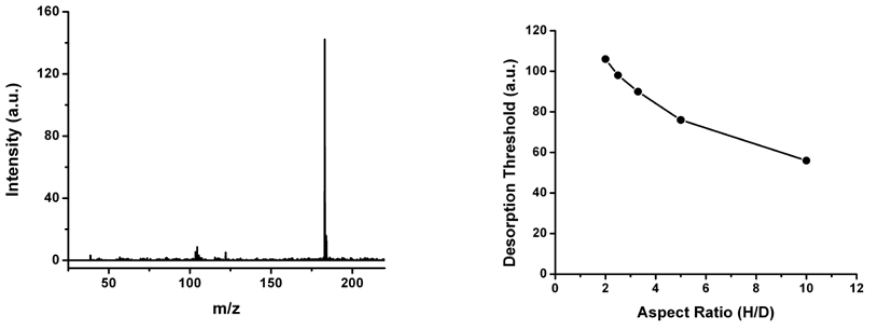

(a) **(b)**

FIGURE 2. (a) Mass spectrum showing the 4M thermometer ion and negligible amount of fragments at the threshold laser fluence. (b)Threshold laser fluence required to desorb ions from NAPA of increasing aspect ratios, H/D, shows a declining trend.

As the fragmentation of the thermometer ion reflects elevated surface temperatures of the substrate and at the fragmentation threshold fluence their decomposition is negligible, it is thought that the related surface temperatures are below the value required for fragmentation. Thus, the decrease in the desorption threshold for higher aspect ratios is not the consequence of elevated temperatures and this effect can be viewed as the direct manifestation of enhanced near fields for higher H/D.

A near-field equivalent of the "shadowing effect," that is observed in the far-field for macroscopic objects, may also occur in the case of nanoscopic structures.[21] In NAPA and LISMA this shadowing effect may be present if the periodicity of the structures is too small or if the structures are too tall.

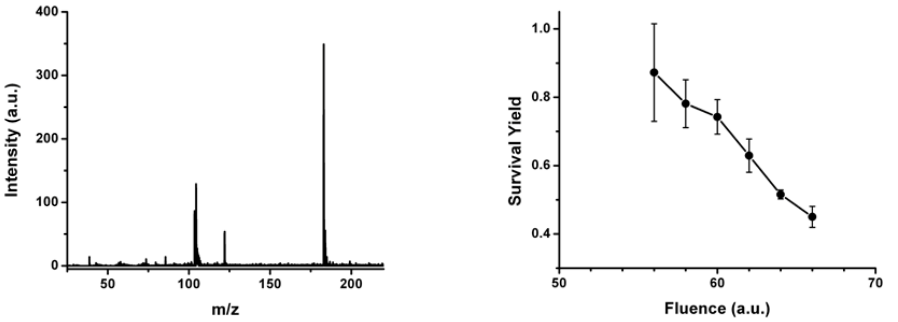

(a) **(b)**

FIGURE 3. (a) Mass spectrum showing the fragmentation channels of the 4M thermometer ion at a laser fluence above the threshold. (b) As the laser fluence increases the survival yield of the 4M ions desorbed from NAPA declines.

Similar to near-field fluorescence experiments where shadowing results in a decrease in fluorescence, in nanophotonic ion sources shadowing may reduce the desorption yields.

In thin posts, e.g., D = 100 nm, additional enhancement of the desorption rate at a given fluence level can be attributed to higher surface temperatures resulting from energy confinement. When the diameter of the posts falls below the thermal diffusion length, the dissipation of the deposited laser energy through heat conduction is hindered. This results in elevated surface temperatures.[26] In the mass spectra of the 4M thermometer ion (see fig. 3a), this effect is manifested in reduced survival yields, the fraction of ions that remains intact, at elevated fluences (see fig. 3b). Although this phenomenon is not the result of a nanophotonic interaction, due to the post dimensions that exhibit such effects, the energy confinement is often observed in the corresponding structures.

ION GENERATION FROM NANOPHOTONIC ION SOURCES

The desorption and ion formation from molecules in MALDI has been studied extensively.[27, 28] The most comprehensive models with predictive power rely on the fluid dynamics[29] or molecular dynamics[30] of the plume expansion and photophysical processes in the plume.[31] In nanophotonic ion sources, the energy deposition, redistribution and plume formation processes are radically altered due to the interactions of the electromagnetic wave with the nanostructure. This results in plume dynamics and ion production processes different from conventional laser ionization sources. For comparison, the physical characteristics of MALDI plume expansion are revisited.

During the UV laser pulse in MALDI, the organic solid matrix absorbs the energy resulting in a phase transition that produces a rapidly expanding plume.[29] Above a laser fluence threshold of $\sim 2\times10^{6}$ W cm^{-2}, neutrals and ions are produced in a highly non-linear process[8] with an ion-to-neutral ratio of 10^{-3} to 10^{-5}.[32, 33] Due to the rapid expansion, plume temperatures drop significantly resulting in the stabilization of the embedded analyte molecules and ions. Above the ionization threshold, the ion yield, Y, as a function of fluence, F, follows a power law, $Y \propto F^{n}$, with an exponent of n = 4 to 6.[8, 34, 35]

As the ejected plume expands, the velocity distributions of the ejected analyte ions[36] and neutrals[37] are independent of their molecular weight. However, it is important to note that the matrix ions in the plume are 100 to 200 m/s faster than the released analyte molecular ions.[38, 39] The angular distribution of the analyte ions exhibits extreme forward directionality. For the exponent of the $\cos^{m}(\theta)$ distribution a range of values up to m = 28 are found in the literature.[40] Surprisingly, the angular distributions of the matrix and analyte particles are significantly different.[41] It was found that large biomolecules have a very narrow angular distribution which becomes "sharpened" or more pronounced over time, whereas the matrix expands radially as well as axially. This "sharpening" was explained in terms of the lack of radial friction interaction of the biomolecules with the radially expanding matrix.

During the MALDI plume formation and expansion, numerous secondary ion-molecule reactions can occur. Proton transfer reactions, from the protonated matrix to a neutral analyte of high proton affinity, are the most common. For analytes with low proton affinities, such as synthetic polymers, alkali cation transfer may take place. Electron transfer reactions lead to radical analyte cations, which are observed for molecules with low polarity.

Of possible relevance to nanophotonic ion sources is the emission of electrons from metallic substrates, due to the photoelectric effect, and their reactive scattering in the MALDI plume.[42] These reactions can reduce the positive charge of the analyte, produce negative ions from neutral molecules with a high electron affinity, or yield more positive ions via electron impact ionization.

Ion production in nanophotonic ion sources, such as LISMA and NAPA, proceeds through different mechanisms. While in MALDI the matrix plays an important role in the protonation of the analyte, in these ion sources produced from silicon there is no obvious source of protons. In the case of LISMA produced by laser surface processing in an aqueous environment, the silicon surfaces are terminated by hydroxyl groups. When irradiated by the desorption laser, these surfaces could donate protons to the analyte. Another potential proton source is the residual solvent entrapped in the troughs of the LISMA structure.

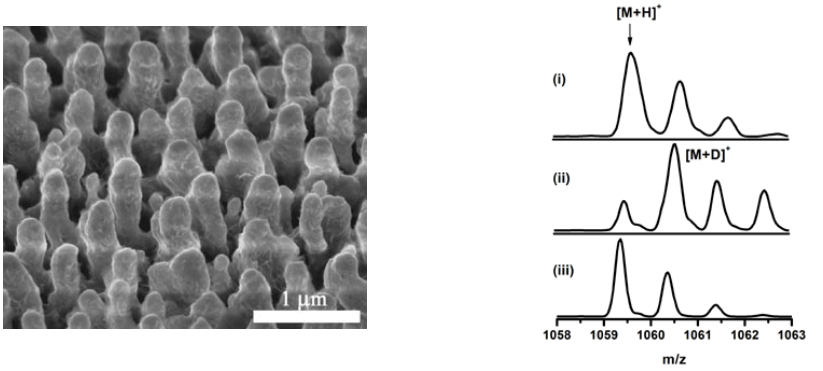

(a) **(b)**

FIGURE 4. (a) SEM image of LISMA showing the columnar structure and the troughs that retain solvent residues. (b) Bradykinin molecular ion production from LISMA produced in H_2O and D_2O environment (i) and (iii), respectively, results in protonated species. In both cases the solvent of the analyte is H_2O. For panel (ii), the LISMA is produced in H_2O but the solvent of the analyte is D_2O. This results in the formation of deuterated molecular ions indicating the role of residual solvent in the ionization process.

To help solve this dilemma, LISMA substrates were produced in H_2O and D_2O environments (fig. 4a). Bradykinin analyte solutions were made in H_2O and D_2O solvents. Laser desorption ionization experiments were conducted by depositing aqueous bradykinin solution onto LISMA produced in the two processing environments (see panels (i) and (iii) in fig. 4b). In the corresponding spectra, protonated bradykinin molecule was observed irrespective of the silicon processing medium. When bradykinin dissolved in D_2O was deposited onto LISMA produced in

aqueous environment, the observed molecular ion was shifted up by one mass unit indicating the role of the residual D_2O in the ionization process (see panel (ii) in fig. 4b).

This evidence is not complete, because it neglects the possible hydrogen-deuterium exchange process in the nanostructures. Further insight has been obtained by derivatizing the LISMA and NAPA structures using silane chemistry. When the hydroxyl groups are exchanged with perfluorophenyl units, no exchangeable hydrogen is left on the surface. To complete the derivatization process, these structures are also baked that further drives the condensed water out of the nanopores. These surfaces still produce protonated analyte species, exhibit lower fluence thresholds and induce less fragmentation.

Additionally, whereas LISMA are created in an aqueous environment, NAPA are produced in vacuum using reactive ion etching. Thus the NAPA surfaces, at least initially, are not covered by hydroxyl groups. Although in the ambient this changes fairly quickly, the degree of coverage should be different from that of LISMA. Yet, the yields of protonated species from NAPA are similar or higher than those from LISMA. Based on the aggregate of these observations, we conclude that the origin of protons in the LISMA and NAPA experiments is the residual solvent entrapped in the silicon structure.

During the illumination of these columnar structures with the desorption laser, other potential ionization processes can be present due to the strong electric fields at the top of the posts. These fields are the product of the near-field enhancement effect close to the post surfaces. Analyte adsorbates subjected to these fields can be stripped of an electron resulting in the formation of a radical cation. The efficiency of these processes is dependent on the nanostructure dimensions. Ion formation can be the product of several other processes. For example, electrons emitted from the silicon can react with the plume;[42] adsorbate-surface collisions can produce ions;[15] and surface hydroxides and hydrides can act as proton sources for ionization.[43]

The plume formed from the residual solvent is highly confined within the nanostructure. Compared to three-dimensional plume expansion observed in MALDI, the confinement in the nanostructure results in a dense plume with quasi-one-dimensional expansion.[44] The confinement of the plume is a function of the nanostructure morphology, and a more restricted volume yields a denser plume with faster reactions in it for a longer period of time.

In light of the above mentioned physical processes contributing to desorption and ionization, the characteristics of the ions produced by nanophotonic sources are discussed in detail below. The abundance and type of ions, the dependence of ion yields on the polarization, the angle of incidence, and the post geometry are compared to the behavior of conventional laser desorption ionization sources.

Abundance and Types of Ions

Analogous to MALDI, for LISMA and NAPA laser fluence thresholds for ionization exist. The ion yields, Y, above this threshold as a function of laser fluence, F, follow a power law relationship, $Y \propto F^n$. In fig. 5a the fluence dependence of the

ion yields of the 4M thermometer ions and the substance P peptide from NAPA (D = 150 nm, H = 1000 nm and P = 337 nm) are compared to the yields of the same ions produced by MALDI from α-cyano-4-hydroxycinnamic acid (CHCA) matrix on a log-log scale. While both processes are strongly non-linear, for the peptide the NAPA system exhibits an exponent of $n \approx 7$ that is significantly higher than the $n \approx 5$ for MALDI. It is worth noting that the fluence dependence of the 4M thermometer ion yields exhibits an exponent of $n \approx 4$ for both NAPA and MALDI. As the thermometer ions are already present in the solid phase, the corresponding ion yields only reflect the efficiency of their desorption. In contrast, the substance P species has to undergo both desorption and ionization. Therefore the higher exponent for NAPA ion yields compared to MALDI is likely related to the ionization process.

It has been demonstrated that positive molecular and quasi-molecular ions can be produced for a range of small biomolecules by nanophotonic ion sources. Similar to MALDI, negative ions can also be generated from NAPA structures. The spectrum of citric acid in fig. 5b produced from NAPA, with a post diameter, periodicity, and height of 175, 575, and 1000 nm, respectively, shows the deprotonated molecular ion as the base peak along with minor fragment ions.

The abundance of the ions produced from nanophotonic ion sources can vary depending on the dimensions of the structure, but are typically somewhat lower than the intensities observed in MALDI for the same laser fluence. For example, the yield of substance P quasi-molecular ions from NAPA (D = 150 nm, H = 1250 nm, P = 400 nm) is ~30% of the yield produced by MALDI from CHCA matrix.

Unique to nanophotonic ion sources, structure specific fragmentation is observed as the laser fluence is increased.[12] In contrast, an additional ion activation step is necessary to induce fragmentation in MALDI. Moreover, both low and high-energy fragmentation channels are active in nanophotonic ion sources.[15]

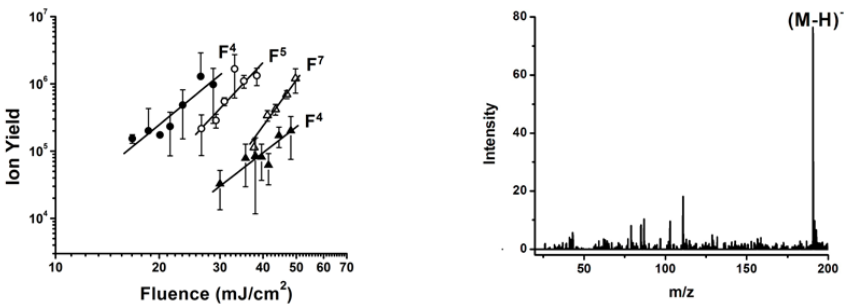

(a) **(b)**

Figure 5. (a) Comparison of the ion yield vs. fluence relationship for MALDI (substance P (○) and 4M thermometer ions (●) from CHCA matrix) and for NAPA with D = 150 nm, H = 1000 nm and P = 337 nm dimensions (substance P (△) and 4M thermometer ions (▲)) ion production. (b) Negative ion mass spectrum of citric acid from NAPA with D = 175 nm, P = 575 and H = 1000 nm.

Polarization and Incidence Angle Dependence

It has recently been discovered that the ion yields from LISMA and NAPA structures show a strong polarization dependence.[14, 16] As the plane of polarization is rotated from p-polarized to s-polarized, the ion yields dramatically diminish, often reaching zero. This phenomenon is absent in MALDI and other laser ionization experiments. For nanophotonic ion sources, a similarly strong dependence on the incidence angle of the laser beam is observed, whereas ion generation from MALDI shows no such behavior.[45]

This unique behavior is explained by the directionality of the columns and posts in LISMA and NAPA, respectively. The projection of the electric field in the laser beam onto the axes of the silicon protrusions generates an axial current in the structure that results in dissipative heating. Rotating the plane of polarization from p- to s-polarized reduces the axial component of the electric field, and thus the dissipative heating, to zero. Similarly changing the incidence angle from, e.g., 45°, to normal incidence reduces the axial component of the electric field. It appears that only the axial component of the electric field promotes ion production. The maximum surface temperature of the nanostructures and the rate of energy dissipation depend on the dimensions of the structures, and the silicon material parameters, such as the resistivity and the heat conductivity. The lack of polarization dependence in MALDI experiments can be explained by the random orientation of the crystallites and the insulating nature of the organic matrix material.

Ion Yield Resonances

NAPA can be tailored to study the interplay between the electromagnetic field and the nanostructure dimensions. Similar to resonances observed in optical antennas, resonant ion yields are observed from nanophotonic ion sources.[16] More specifically, for subwavelength post diameters with high aspect ratios, ion yield gains of up to 55 are detected. This is attributed to the electric field enhancement, κ in equation 1, in the vicinity of the posts. Similar to near-field fluorescence measurements, as the diameter of the posts decreases, the resonant aspect ratio increases. [20] Periodicity only has a minor effect, indicating that the interaction between the posts, i. e., the array effect, is minimal.

DIMENSIONS AND SURFACE CHEMISTRY

In MALDI experiments the most essential parameters determining the yields and internal energies of ions are the choice of the matrix material, and the wavelength and fluence of the laser radiation. While the latter two are important in nanophotonic ion sources as well, the dimensions of the structure and the physical and chemical properties of the surface are also significant.

Nanostructure Dimensions

To investigate the role of the nanostructure dimensions on the ionization efficiency, post diameters, periodicities, and heights of NAPA are varied from 50 to 600 nm, 200 to 1200 nm, and 200 to 1500 nm, respectively. Resonant ion yields with high gains for large aspect ratio posts are detected and have already been mentioned in the Ion Yield Resonances section. However, it is important to note the influence of each of these parameters on the ion yields separately.

At a given fluence, thin posts produce higher ion yields than their thick counterparts. The threshold fluence for ion generation is also lower for slender structures. As mentioned above, this is explained in terms of energy confinement in structures thinner than the thermal diffusion length. As a consequence, the surface temperatures of these posts sharply increase with decreasing diameter. This results in enhanced energy transfer to the analyte, higher ion yields and internal energies. However, upon further increasing the fluence in these posts other physical processes can become dominant. For example, transient melting is observed at ~30 mJ/cm^2 laser fluence for post diameters smaller than 100 nm.[16] Further reducing the nanopost diameters to length scales smaller than the phonon mean free path changes the heat transport mechanism from purely diffusive to ballistic-diffusive, and eventually ballistic, resulting in altered temperature profiles.

The post height plays an analogous role to the length in optical antennas. In the case of NAPA, ion yields increase with the post height within the range of 200-1200 nm. However, a significant drop is observed in ion abundance at a height of 1500 nm. In near-field fluorescence measurements a similar decrease in the intensity enhancement factor is observed at a normalized probe length of ~12.[20] This decline is explained in terms of the electromagnetic resonances within the probe tip diminishing the evanescent field.

Of the three varied parameters, the periodicity has the least significant impact on the ion yields. Only a marginal dependence is observed, where larger periodicities produce slightly higher ion yields. This indicates that the localized field enhancements around the posts contribute to desorption and ionization and the shadowing effect is detrimental to the production of ions.

Surface Chemistry

While the dimensions of the nanostructures significantly impact ion yields, their surface chemistry can also influence the ionization efficiency. For example, the surfaces properties of LISMA and NAPA can be modified by derivatization through silane chemistry. Not only does this alter the chemical properties of the surface, but also its hydrophobicity. Derivatization with (pentafluorophenyl) propyldimethylchlorosilane results in enhanced ion yields and, for LISMA, higher internal energy values than the native surface.[15] Surface derivatization can lower the threshold laser fluence, result in increased ion yields, and alter the exponent in the power law connecting ion production to the laser fluence. These findings indicate that

as the nanostructure-adsorbate interaction energy decreases, ion production can become more efficient.

FUTURE DIRECTIONS

In this paper we have established the basic properties of nanophotonic ion sources and have described their interactions with the electromagnetic radiation. The ability of these nanostructures to exhibit localized electromagnetic resonances results in novel ways of producing ions. We have demonstrated how these interactions can be utilized in laser desorption and ionization experiments, and shown how ion yields can be influenced by the physical and chemical properties of these nanophotonic structures.

The power to shape the laser light-nanostructure interaction through structural properties and to efficiently optimize the resulting enhanced ion yields is unique to nanophotonic ion sources. Beyond their obvious use for ion production in mass spectrometry, they are candidates for energy harvesting and as solar cell materials. In addition, due to their small dimensions, these sources are amenable for integration with microfluidic separation devices and miniaturized mass spectrometers.

ACKNOWLEDGMENTS

The authors appreciate the financial support from the Chemical Sciences, Geosciences and Biosciences Division, Office of Basic Energy Sciences, Office of Science, U.S. Department of Energy (DE-FG02-01ER15129). Support from the Department of Energy does not constitute an endorsement of the views expressed in the article. Scholarship awards from the Achievement Rewards for College Scientists Foundation, Inc. (ARCS) to J.A.S. and B.N.W. are greatly appreciated. NAPA were nanofabricated in the framework of a User Agreement (CNMS2008-249) at Oak Ridge National Laboratory's Center for Nanophase Materials Sciences, sponsored by the Scientific User Facilities Division, Office of Basic Energy Sciences, U.S. Department of Energy. Some of the authors (B. N. W. and J. A. S.) would like to thank S. T. Retterer and D. L. Pickel of the Oak Ridge National Laboratory for training and helping with the production of the NAPA structures.

REFERENCES

1. G. Wedler and H. Ruhmann, *Surface Science*, **121**(3), 464-486 (1982).
2. C. Simpson and J.P. Hardy, *Chemical Physics Letters*, **130**(3), 175-180 (1986).
3. G.Y. Chen and E.S. Yeung, *Analytical Chemistry*, **60**(9), 864-868 (1988).
4. L. Balazs, R. Gijbels, and A. Vertes, *Analytical Chemistry*, **63**(4), 314-320 (1991).
5. S. Georgiou and A. Koubenakis, *Chemical Reviews*, **103**(2), 349-393 (2003).
6. K.W. Tanaka, H.; Ido, Y.; Akita, S.; Yoshida, Y.; Yoshida, T., *Rapid Communications in Mass Spectrometry*, **2**(8), 151-153 (1988).
7. M. Karas and F. Hillenkamp, *Analytical Chemistry*, **60**(20), 2299-2301 (1988).

8. W. Ens, Y. Mao, F. Mayer, and K.G. Standing, *Rapid Communications in Mass Spectrometry*, **5**(3), 117-123 (1991).
9. S.A. Akhmanov, V.I. Emelyanov, N.I. Koroteyev, and V.N. Seminogov, *Uspekhi Fizicheskikh Nauk*, **147**(4), 675-745 (1985).
10. T.H. Her, R.J. Finlay, C. Wu, S. Deliwala, and E. Mazur, *Applied Physics Letters*, **73**(12), 1673-1675 (1998).
11. A.J. Pedraza, J.D. Fowlkes, and D.H. Lowndes, *Applied Physics Letters*, **74**(16), 2322-2324 (1999).
12. Y. Chen and A. Vertes, *Analytical Chemistry*, **78**(16), 5835-5844 (2006).
13. C. Wu, et al., *Applied Physics Letters*, **78**(13), 1850-1852 (2001).
14. B.N. Walker, T. Razunguzwa, M. Powell, R. Knochenmuss, and A. Vertes, *Angewandte Chemie-International Edition*, **48**(9), 1669-1672 (2009).
15. J.A. Stolee, Y. Chen, and A. Vertes, *The Journal of Physical Chemistry C*, **114**, 5574-5581 (2010).
16. B.N. Walker, J.A. Stolee, D.L. Pickel, S.T. Retterer, and A. Vertes, *The Journal of Physical Chemistry C*, **114**, 4835-4840 (2010).
17. D.A. Kossakovski, S.D. O'Connor, M. Widmer, J.D. Baldeschwieler, and J.L. Beauchamp, *Ultramicroscopy*, **71**(1-4), 111-115 (1998).
18. R. Stockle, P. Setz, V. Deckert, T. Lippert, A. Wokaun, and R. Zenobi, *Analytical Chemistry*, **73**(7), 1399-1402 (2001).
19. H.F. Hamann, A. Gallagher, and D.J. Nesbitt, *Applied Physics Letters*, **76**(14), 1953-1955 (2000).
20. J.L. Bohn, D.J. Nesbitt, and A. Gallagher, *Journal of the Optical Society of America a-Optics Image Science and Vision*, **18**(12), 2998-3006 (2001).
21. H.F. Hamann, M. Kuno, A. Gallagher, and D.J. Nesbitt, *Journal of Chemical Physics*, **114**(19), 8596-8609 (2001).
22. Y. Wang, et al., *Applied Physics Letters*, **85**(13), 2607-2609 (2004).
23. J. Merlein, M. Kahl, A. Zuschlag, A. Sell, A. Halm, J. Boneberg, P. Leiderer, A. Leitenstorfer, and R. Bratschitsch, *Nature Photonics*, **2**(4), 230-233 (2008).
24. P. Muhlschlegel, H.J. Eisler, O.J.F. Martin, B. Hecht, and D.W. Pohl, *Science*, **308**(5728), 1607-1609 (2005).
25. H. Fischer and O.J.F. Martin, *Journal of the European Optical Society-Rapid Publications*, **3**, 4 (2008).
26. M. Sadeghi and A. Vertes, *Appl. Surf. Sci.*, **127-129**, 226-234 (1998).
27. K. Dreisewerd, *Chemical Reviews*, **103**(2), 395-425 (2003).
28. R. Zenobi and R. Knochenmuss, *Mass Spectrometry Reviews*, **17**(5), 337-366 (1998).
29. A. Vertes, G. Irinyi, and R. Gijbels, *Analytical Chemistry*, **65**(17), 2389-2393 (1993).
30. A. Bencsura and A. Vertes, *Chemical Physics Letters*, **247**(1-2), 142-148 (1995).
31. R. Knochenmuss, *Journal of Mass Spectrometry*, **37**(8), 867-877 (2002).
32. C.D. Mowry and M.V. Johnston, *Rapid Communications in Mass Spectrometry*, **7**(7), 569-575 (1993).
33. A.A. Puretzky and D.B. Geohegan, *Chemical Physics Letters*, **286**(5-6), 425-432 (1998).
34. K. Dreisewerd, M. Schurenberg, M. Karas, and F. Hillenkamp, *International Journal of Mass Spectrometry and Ion Processes*, **154**(3), 171-178 (1996).
35. G. Westmacott, W. Ens, F. Hillenkamp, K. Dreisewerd, and M. Schurenberg, *International Journal of Mass Spectrometry*, **221**(1), 67-81 (2002).
36. R.C. Beavis and B.T. Chait, *Chemical Physics Letters*, **181**(5), 479-484 (1991).
37. T. Huthfehre and C.H. Becker, *Rapid Communications in Mass Spectrometry*, **5**(8), 378-382 (1991).
38. P. Juhasz, M.L. Vestal, and S.A. Martin, *Journal of the American Society for Mass Spectrometry*, **8**(3), 209-217 (1997).
39. X.W. Wu, M. Sadeghi, and A. Vertes, *Journal of Physical Chemistry B*, **102**(24), 4770-4778 (1998).
40. W. Zhang and B.T. Chait, *Int. J. Mass Spectrom. Ion Processes*, **160**(1-3), 259-267 (1997).

41. A.A. Puretzky, D.B. Geohegan, G.B. Hurst, M.V. Buchanan, and B.S. Luk'yanchuk, *Physical Review Letters*, **83**(2), 444-447 (1999).
42. V. Frankevich, R. Knochenmuss, and R. Zenobi, *International Journal of Mass Spectrometry*, **220**(1), 11-19 (2002).
43. S.M. Prokes, O.J. Glembocki, V.M. Bermudez, R. Kaplan, L.E. Friedersdorf, and P.C. Searson, *Physical Review B*, **45**(23), 13788-13791 (1992).
44. G.H. Luo, Y. Chen, G. Siuzdak, and A. Vertes, *Journal of Physical Chemistry B*, **109**(51), 24450-24456 (2005).
45. A. Westman, T. Huthfehre, P. Demirev, J. Bielawski, N. Medina, and B.U.R. Sundqvist, *Rapid Communications in Mass Spectrometry*, **8**(5), 388-393 (1994).